The age and genesis of the Nifty copper deposit: back to the future

GEOSCIENCE AUSTRALIA
PROFESSIONAL OPINION 2007/03

by

David L. Huston[1], Roland Maas[2] and Karol Czarnota[1]

1. Geoscience Australia, GPO Box 378, Canberra, ACT 2601
2. School of Earth Sciences, The University of Melbourne, VIC 3010

Department of Industry, Tourism & Resources
Minister for Industry, Tourism & Resources: The Hon. Ian Macfarlane, MP
Parliamentary Secretary: The Hon. Bob Baldwin, MP
Secretary: Mark Paterson

Geoscience Australia
Chief Executive Officer: Dr Neil Williams

GeoCat # 65044

Bibliographic reference: Huston, D. L., Maas, R. and Czarnota, K., 2007. The age and genesis of the Nifty copper deposit: back to the future. Geoscience Australia Professional Opinion, 2007/03, 22pp.

Contents

Executive Summary

A Nd-Sm isochron from apatite in apatite-chalcopyrite veins mostly in the footwall to the Nifty deposit indicates an age of 791 ± 43 Ma. As this apatite is paragenetically associated with chalcopyrite in the veins and in the ore zone, this age is interpreted as the best estimate for the timing of mineralisation at the Nifty deposit. Consideration of the temporal evolution of ε_{Nd} values precludes deposition of the apatite significantly younger than 800 Ma. The U-Pb systematics of the apatite have been disturbed, resulting mostly in highly scattered arrays that do not have geologic significance.

Observations on primary fluid inclusions in quartz from the apatite veins suggest low temperature, relatively high salinity brines. These observations, the geochronological constraints and large ranges in sulphur isotope values suggest that the Nifty deposit formed early, possibly diagenetically, from low temperature, relatively oxidised fluids. This inference is consistent with the original model for the Nifty deposit (Haynes et al., 1993) though less consistent with the tectonic model proposed by Anderson et al. (2001).

Structural modelling assuming that mineralisation is early shows that the north trend of ore shoots reported previously on the northeastern limb of the Nifty Anticline is consistent with control by antithetic normal faults developed during basin formation. If this model is correct, these antithetic normal faults would trend west-southwest on the southwestern limb of the Nifty Anticline. This trend has not been adequately drill-tested, and provides scope for additional near-mine exploration on the southwestern limb of the Nifty Anticline.

Introduction

After the Telfer gold deposit, the Nifty copper deposit is the most significant ore deposit in the Neoproterozoic Paterson Region of Western Australia (Fig. 1). This deposit was discovered in the early 1980s by WMC Resources Ltd using a sediment-hosted stratiform copper exploration model in which copper was sourced from mafic volcanic rocks and deposited diagenetically in fine grained siliciclastic rocks (Haynes et al., 1993). However, based on structural and paragenetic timing relationships Anderson et al. (2001) suggested that the deposit formed at ca. 717 Ma, at least 100 million years after the deposition of the host sediments. They inferred that hydrothermal fluids were driven from deep in the Yeneena Basin along thrusts to the carbonaceous and dolomitic siltstones where copper was deposited.

Our own observations confirmed a very strong structural control on copper mineralisation, with the orebody concentrated along the northeastern, steep limb of a syncline (Fig. 2) that has an orientation

consistent with formation during the ca. 650 Ma Miles Orogeny. Moreover, chalcopyrite is closely associated with a moderately to strongly developed fabric that is axial plan to this fold (Fig. 3a), leading us to initially concur with the model of Anderson et al. (2001).

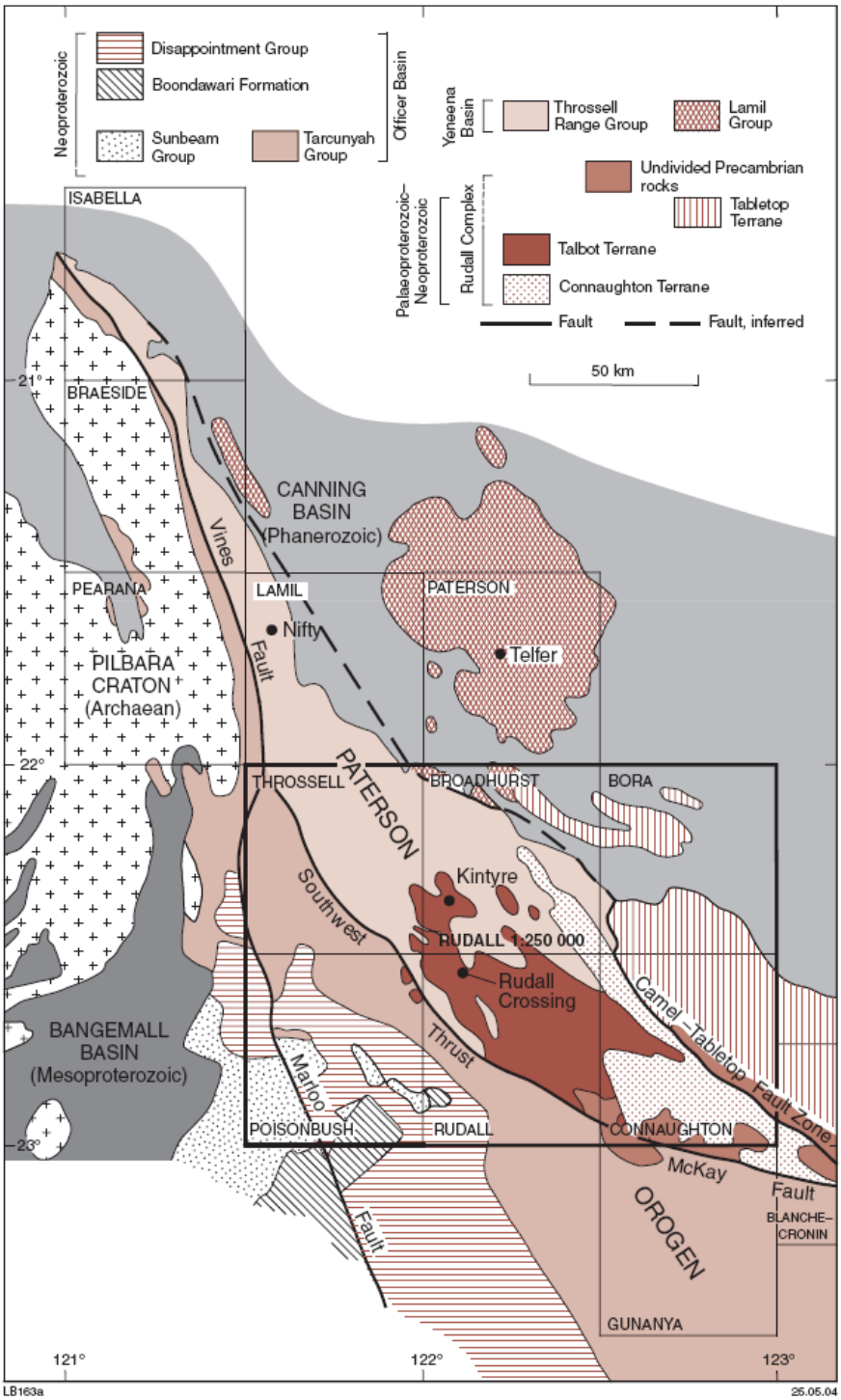

Figure 1: *Regional geology of the Paterson region showing the location of the Nifty deposit (after Bagas, 2004).*

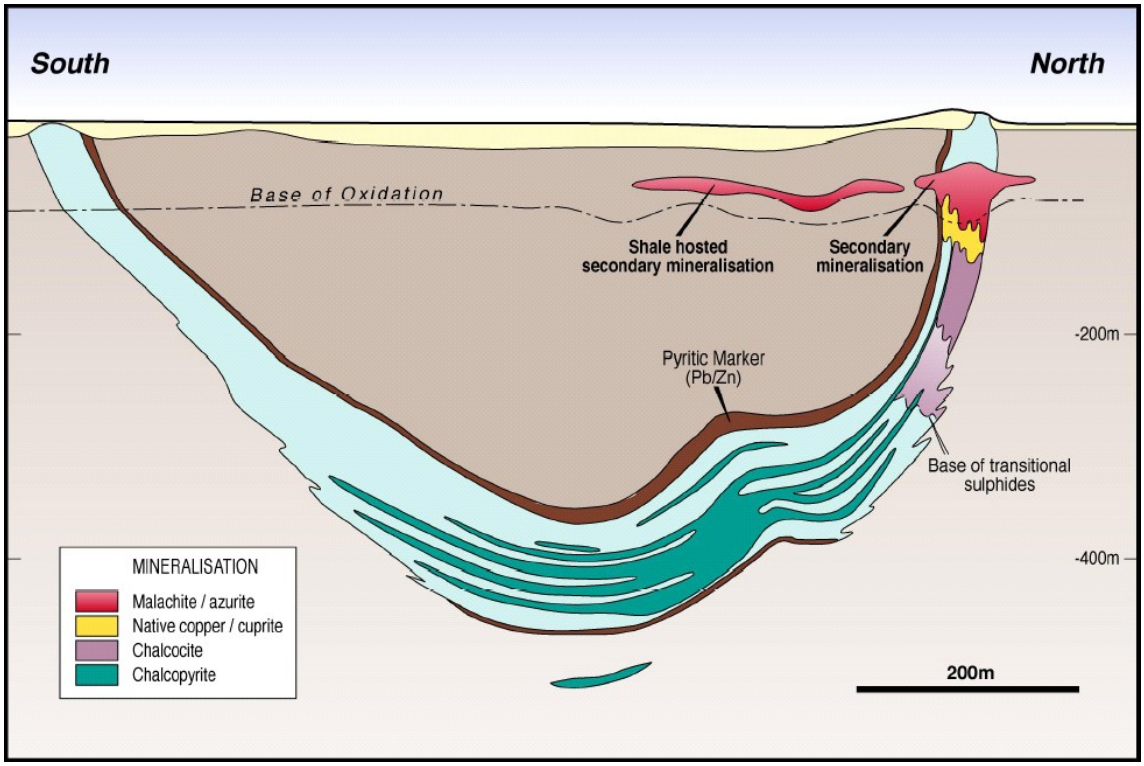

Figure 2: *Cross section of the Nifty deposit (after Straits Resources website).*

To critically test the alternative genetic models for Nifty, a geochronological program was designed to establish the ages of mineralisation and of the host Broadhurst Formation. This report presents age constraints for the Cu mineralisation obtained from Sm-Nd and U-Pb isotope studies of hydrothermal apatite extracted from chalcopyrite-bearing apatite veins in the structural footwall to the deposit, and from U-Pb data for chalcopyrite and associated strongly altered host rock. Initial Sr-Nd isotope data for the apatites are used to examine possible pathways/metal sources of the hydrothermal fluid. The results from this work are compared with age constraints for the Broadhurst Formation and discussed in terms of models for ore formation and exploration.

Regional Geology

The Nifty deposit is hosted by the Neoproterozoic Yeneena Supergroup of the Paterson Orogen (Bagas, 2004). The Yeneena Supergroup unconformably overlies Mesoproterozoic metamorphosed sedimentary and igneous rocks of the Rudall Metamorphic Complex. Bagas (2004) subdivided the Yeneena Supergroup into the Throssell Range Group and the Lamil Group. The Throssell Range Group comprises three units, the Coolbro Sandstone, a quartzose sandstone with basal conglomerate, the Broadhurst Formation, a carbonaceous shale/siltstone unit that hosts the Nifty deposit, and the Isdell Formation, a carbonate dominated unit.

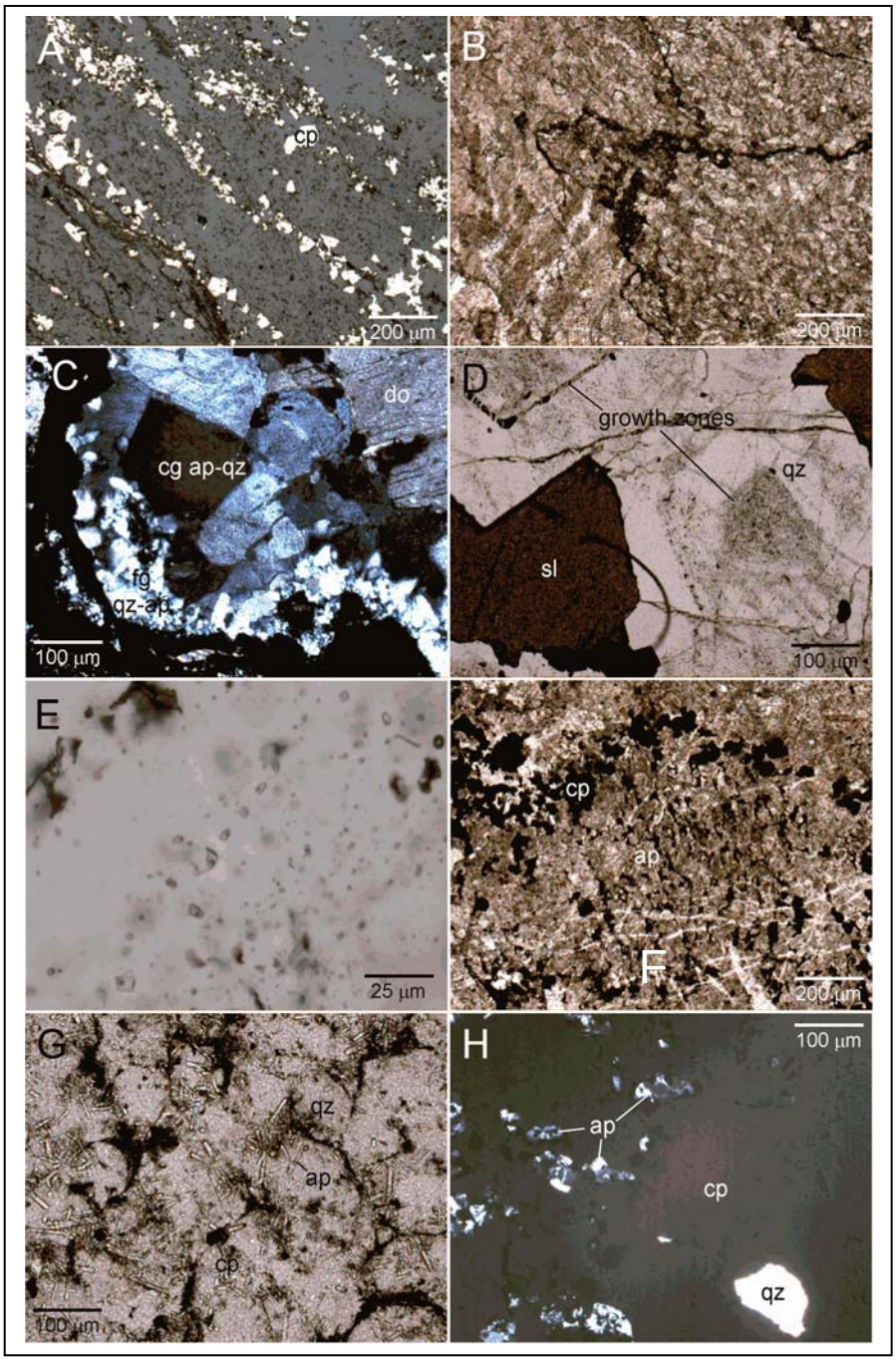

Figure 3: *Photomicrographs showing ore textures at the Nifty deposit. (A) Chalcopyrite (cp) developed along foliation interpreted to have formed during the Miles Orogeny (reflected light. (B) Stylolitic disordered carbon veins in microcrystalline dolostone (transmitted light). (C) Margin of apatite vein showing an outer fine-grained quartz-apatite assemblage (fg qz-ap) infilled by coarser-grained apatite-quartz (cg ap-qz) assemblage and then by dolomite (do; transmitted light, crossed nichols). (D) Dolomite-sphalerite (sp)-quartz assemblage filling late-stage open space in apatite veins (transmitted light). Note growth zones in quartz. (E) Liquid-rich fluid inclusions decorating growth zones in quartz within late-stage open space fill (transmitted light). (F) Apatite-chalcopyrite assemblage that has replaced microcrystalline dolostone (transmitted light). (G) Unoriented, acicular apatite grains in quartz-chalcopyrite assemblage from ore zone (transmitted light). (H) Inclusions of apatite and quartz in semi-massive chalcopyrite from ore zone (transmitted light, crossed nichols).*

Neoproterozoic rocks of the Yeneena Supergroup have been affected by two deformation events, the earlier Miles Orogeny, which is characterised by north-northwest-trending folds and thrust faults, and the later Paterson Orogeny, which reactivated earlier structures (Bagas, 2004), resulting in dextral slip along the Vines Fault. The ages of both of these events are poorly constrained and may be progressive. Bagas (2004) inferred a ca. 720 Ma age for the Miles Orogeny based on a possible correlation with the Areyonga tectonic movement in the Amadeus Basin, whereas Durocher et al. (2003) inferred an age range of 680-630 Ma for the Miles Orogeny based on ^{40}Ar-^{39}Ar ages from the Throssell Range Group. This age range corresponds to a major period of felsic plutonism (the Mount Crofton Suite) at c. 650 Ma (Dunphy and McNaughton, 1998). The age of the Paterson Orogeny inferred by Bagas (2004) at ca. 550 Ma is supported by ^{40}Ar-^{39}Ar ages reported by Durocher et al. (2003). In addition to granites of the Mount Crofton Suite, the Broadhurst Formation was intruded by a suite of mafic to intermediate sills and plutons at ca. 830-816 Ma (see below).

Geology of the Nifty deposit

The Nifty deposit is a series of broadly stratiform lenses localised within the Broadhurst Formation near the closure of a south-southeast-plunging, open to tight syncline (Figs. 2 and 4). The host sequence consists dominantly of chloritic, carbonaceous and locally pyritic shale with localised lenses of dolostone. According to Anderson et al. (2001), the immediate ore host, the Nifty member, contains interbedded dolomitic mudstone with the carbonaceous shale. Immobile trace element analyses suggest that the ore is associated with silicified dolostone (D Huston, unpub. data).

The ore mineralogy and metallogeny is simple: within primary ore, chalcopyrite is the dominant sulphide mineral and copper is the only metal recovered. In 2000, Straits Resources defined a global resource of 99 Mt grading 1.7% copper. In addition to chalcopyrite, the ores also contain accessory pyrite, and abundant pyrite with accessory to minor sphalerite and galena are present within the Pyrite Marker Bed 1.5-22m-thick unit 20-40m stratigraphically above the Nifty member. In addition to the pyrite and chalcopyrite, the ore zone is characterised by intense silicification with accessory dolomite, carbonaceous material and fluorapatite. Minor to trace minerals in the ore zone include uraninite and pitchblende (Anderson et al., 2001).

Age constraints on the Broadhurst Formation

Although the Broadhurst Formation, which hosts the Nifty deposit, has not been dated directly, its age is constrained by four age determinations from units that underlie, overlie and intrude this unit. Detrital zircon age spectra have been determined for the underlying Coolbro (Nelson, 1995; N

Neumann, 2006, pers. comm.), with the youngest maximum depositional age of ca. 910 Ma reported by Nelson (1995). A detrital spectrum for the Punta Punta Formation, which is located much higher in the stratigraphy yielded a maximum depositional age of ca. 850 Ma. The Coolbro maximum depositional age of ca. 910 Ma is the best constraint on the maximum age of the Broadhurst Formation.

A minimum depositional age is provided by the Duke Monzonite, a mafic sill and an unnamed intermediate to mafic intrusion, which intrude the Broadhurst Formation and have emplacement ages of 831 ± 5 Ma, ca. 830 Ma (D Maidment, pers. comm., 2006) and 816 ± 6 Ma (Reed, 1996), respectively. These data constrain the depositional age of the Broadhust and Coolbro Formations to between ca. 910 and ca. 830 Ma. Using data of Goellnicht (1992), Reed (1996) interpreted a Pb-Pb carbonate isochron age of 807 ± 61 Ma for the Isdell Formation, which overlies the Broadhurst Formation. Although this apparent isochron has a high MSWD (10.4; n = 6), this age, which is best interpreted as a diagenetic age of the Isdell Formation, is consistent with the other data and suggest that the deposition of the Coolbro, Broadhurst and Isdell Formations occurred around 830 Ma.

Paragenesis of apatite veins and relationship with copper mineralisation

Using geochemical data provided by Birla Nifty as a guide, five samples containing apatite (Table 1) were collected for petrographic and geochronological studies. The samples are located at the edge of high grade ore zones (>3% Cu) and silica-dolomite alteration zones, predominantly in the footwall to the deposit (Fig. 4). In most samples, apatite occurs in 2-10 mm stockwork breccia veins (Figs. 5a-c) within carbonaceous shales and siltstones that contain up to 5% framboidal and anhedral pyrite in discrete bands. The apatite veins are typically 2-10 mm in width and contain entrained, angular 1-5 mm wall rock fragments in addition to varying amounts of visible chalcopyrite (Figs. 5a,c,e) and pyrite (Figs. 5a-b). Locally the veins are folded and partly recrystallised (Figs. 5b,d). The development of a planar vein off one of these folded veins (Fig. 5d) may indicate local remobilisation of apatite during deformation. In one sample (2005678049-01: Fig. 5f), however, massive apatite-chalcopyrite rock has replaced primary dolostone, and both are veined by dolomite veins.

In detail, the vein paragenesis is moderately complex. The earliest vein set is stylolitic disordered carbon veins, which are present within both shale/siltstone and dolostone (Fig. 3b). With the exception of sample 2005678050-01, these veins grade into or are obliquely cut by apatite-bearing veins. The margins of the apatite veins are characterised by 0.1-2 mm-thick zones defined by a

quartz-pyrite-apatite assemblage with minor to accessory disordered carbon and rutile (Fig. 3c). The minerals in these zones tend to be relatively fine-grained (0.005-0.1-mm) and, with the exception of apatite, anhedral. Although no discrete uranium minerals were identified in this study, Anderson et al. (2001) cited unpublished WMC data reporting very fine-grained uranitite and pitchblende associated with carbonaceous material.

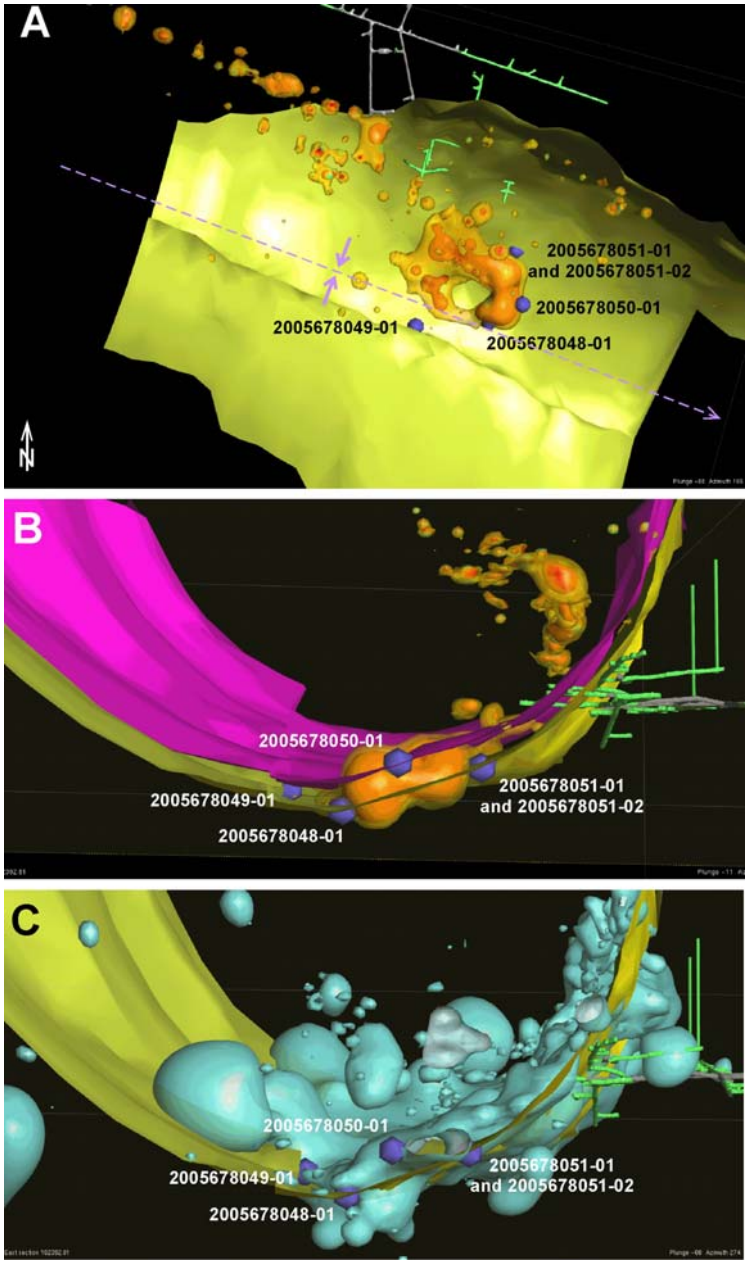

Figure 4: *Diagrams showing the location of samples collected relative to features of the Nifty deposit. (A) Plan view showing the footwall shale wire frame (yellow) and the 3 % and 5% copper ore shells. (B) Cross-sectional view showing the 3% (light orange) and 5% copper (dark orange) ore shells, the top of the footwall shale (yellow) and the top of the middle carbonate surface. (C) Cross sectional view showing the edge of silica-dolomite alteration zones. The yellow surface is the top of the footwall shale.*

Table 1: Apatite samples collected for geochronological study

Drill hole	Depth (m)	U (ppm)	Pb (ppm)	U/Pb	Ca (%)	Cu (%)	Sample	Depth (m)	Description
YNC132	409-410	461	51	9.04	15.50	1.49	7049-01	409.0-409.2	Fractured apatite veins cutting shale. The veins are cut by a fibrous quartz vein.
YNC133	463.3-464.3	989	130	7.61	11.67	1.00	7048-01	463.6-463.8	Apatite-chalcopyrite stringers cutting shale.
YNC136	399-401	1300	220	5.91	5.00	0.08	7051-01	400.0-400.15	Folded, stockwork apatite veins cutting shale.
YNC136	399-401	1300	220	5.91	5.00	0.08	7051-02	400.4-400.6	Large apatite veins cutting shale. The veins are folded, but emplaced along the axial planar crenulation to the fold.
YNC144A	407-408	353	50	7.06	7.93	1.78	7050-01	407.25-407.45	Irregular chalcopyrite-apatite veins cutting shale.

The interiors of the veins are filled by a coarser-grained (0.2-2 mm) assemblage dominated by apatite and quartz with accessory to minor chalcopyrite, pyrite, disordered carbon and sphalerite, variable sericite and dolomite, and trace galena. In section 2005678051-02B the sericite forms in discrete quartz-apatite-sericite veins. Paragenetically, the sulphide minerals and dolomite are last, filling open space within apatite and quartz (Fig. 3d). The sphalerite is relatively pale, indicating a low Fe content (Fig. 3d), and primary fluid inclusions in adjacent growth-zoned quartz have low vapour/liquid ratios and halite (?) daughter minerals, suggesting deposition from low temperature, saline ore fluids (Fig. 3e).

In sample 2005678050-01 massive microcrystalline dolostone (Fig. 3b) has been replaced by texturally similar apatite-chalcopyrite assemblages with minor pyrite and disordered carbon (Fig. 3f). This assemblage and microcrystalline dolomite are cut by a series of 5-15 mm dolomite fibre veins (Fig. 5f) with trace disseminated chalcopyrite and pyrite. The dolomite veins are cut by thin (<2 mm) quartz-dolomite-chalcopyrite veins, and this vein and the carbonate fibre veins are cut by a sheared carbonate-disordered carbon vein with minor pyrite, chalcopyrite and chlorite.

In all of the samples collected for apatite veins, chalcopyrite is paragenetically closely associated with apatite both in veins and replaced dolostone. Moreover, the apatite-chalcopyrite assemblage generally contains disordered carbon and pyrite and may contain minor to trace sericite iron-poor sphalerite, dolomite and galena. Although apatite has not been recognised in veins from the ore zone, Anderson et al. (2001) reported abundant fluorapatite within the black quartz alteration assemblage

closely associated with chalcopyrite-rich ore. Texturally, the apatite is present as unoriented acicular grains up to 200 μm long within an assemblage dominated by lath-like quartz with accessory chalcopyrite and pyrite (Fig. 3g). Apatite is also present as inclusions, along with quartz, dolomite and pyrite within semi-massive chalcopyrite (Fig. 3h). The intimate association of fluorapatite with chalcopyrite in the ore zone, as reported by Anderson et al. (2001) and confirmed by this study, suggests that apatite and chalcopyrite deposition coincided, indicating that ages determined from vein apatite should be indicative of the age of copper mineralisation at Nifty.

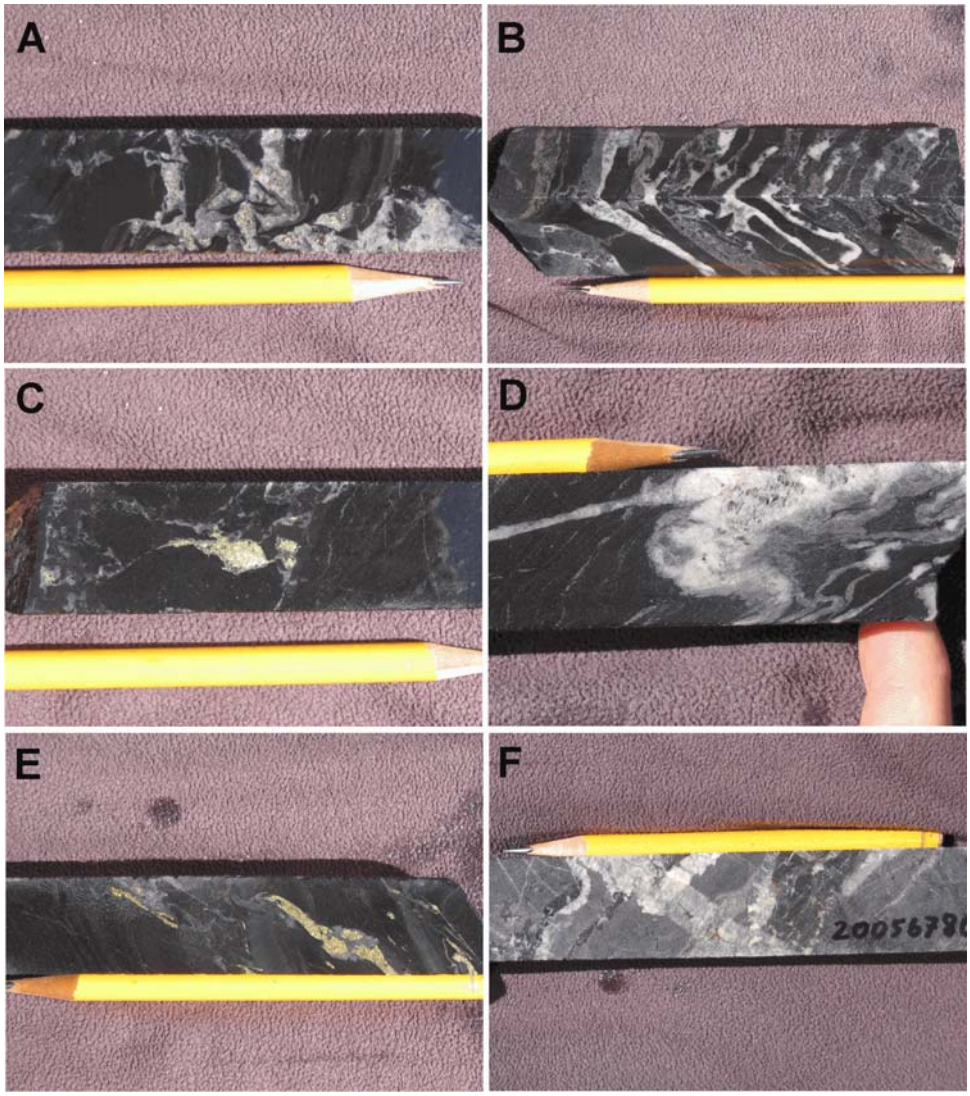

Figure 5: *Photographs of samples used in this study. All veins except (F) cut pyritic and carbonaceous siltstone/shale. (A) Stockwork apatite-chalcopyrite veins (sample 2005678048-01). (B) Stockwork apatite-pyrite veins. Note the folded, pyrite-rich vein in right of photo (sample 2005678051-01). (C) Chalcopyrite segregations in stockwork apatite veins (sample 2005678048-01). (D) Folded apatite-pyrite veins cutting pyritic and carbonaceous siltstone (sample 2005678051-02). (E) Chalcopyrite-apatite veins (sample 2005678050-01). (F) Fibre dolomite veins cutting microcrystalline dolostone. To the left of the sample number, the darker zone is apatite chalcopyrite rock that has replaced dolostone (sample 2005678049-01).*

As part of this study, disordered carbon was identified using laser Raman analysis. These data can also be used to estimate metamorphic temperatures. Using the calibration of Beyssac et al. (2002), the maximum metamorphic temperature at Nifty was about 330°C, although this temperature is at the bottom of the calibration of Beyssac et al. (2002).

Geochronology

Mineral separations were performed on all five samples listed in Table 1. Apatites from two of these samples (2005678048-01, 2005678051-02, henceforth referred to as samples 1 and 2) were used for the geochemical and isotopic work reported here.

ANALYTICAL METHODS

All geochemical and isotopic work was carried out at the School of Earth Sciences, University of Melbourne. Trace element compositions for apatite were determined by solution-mode ICP-MS, using a Varian quadrupole ICPMS, following the procedures of Eggins et al. (1997) and Kamber et al. (2003). For this work, 10 sub-samples comprising 4 - 20 apatite grains were cleaned in very dilute HNO_3 and distilled water, followed by dissolution in strong HNO_3. USGS basalt standard W-2 was used for calibration. Based on the results of this work, 4 apatite sub-samples (weighing ≈ 4-5 mg) from each of the two samples were dissolved in HNO_3 and aliquotted for U-Pb and Sm-Nd/Sr isotope work. For the U-Pb work, an aliquot of 1-1.5 mg was spiked with mixed ^{233}U-^{205}Pb tracer, followed by separation of Pb and U using conventional anion exchange and EICHROM TRU resin, respectively. Total Pb blank was 10 pg. For Sm-Nd work, the remaining sample solutions for 6 samples were spiked with mixed ^{149}Sm-^{150}Nd tracer, followed by extraction of LREE and Sr using EICHROM RE- and SR-resin; Sm and Nd were further purified using EICHROM LN resin. The isotopic analyses were carried out on a NU Instruments multi-collector ICPMS. Mass bias for Pb was corrected by standard bracketing, while Nd and Sr data were corrected by normalizing to $^{146}Nd/^{145}Nd=2.0719425$ (equivalent to $^{146}Nd/^{144}Nd = 0.7219$) and $^{88}Sr/^{86}Sr=8.37521$, respectively (for details, see Maas et al., 2005).

RESULTS

Apatite trace element data

Apatites from each sample show a high degree of compositional homogeneity (Table 2), with fairly narrow ranges of key trace elements such as Sr (410-680 ppm in sample 1; 860-1003 ppm in sample 2), Y (109-168 ppm) and U (101-234 ppm; 21-52 ppm). By contrast, Cu (56-4413 ppm), Zn (11-2518 ppm) and Pb (5-171 ppm) vary strongly, probably reflecting variable contents of sulphide impurities and/or fluid inclusions. Th is low (≤1 ppm), as are the high-field strength (HFS) elements (Ti, Zr, Nb, Hf, Ta); the latter is characteristic of apatite. The rare earth elements (REE) are

dominated by the middle REE (Sm to Dy), and this is reflected in unusual roof-shaped chondrite-normalised REE patterns (Fig. 6). Apatites from both samples have similar patterns with peaks at Gd, but sample 1 apatites have a small negative Eu anomaly which is absent in sample 2 apatites. By contrast, sample 2 apatites show a slope reversal at Ce and thus have much higher $[La/Ce]_{CN}$ ratios. Sm/Nd ratios are high in both samples and thus favorable for Sm-Nd geochronology. U/Pb ratios are also reasonably high but show a large range (0.3-7.9) reflecting highly variable Pb contents.

Sm-Nd and U-Pb isotope data

The Sm-Nd isotopic data for apatite reflect their high Sm/Nd in the form of very radiogenic Nd isotope ratios. However, the samples lack the within-sample dispersion to define precise isochrons from sub-samples of individual samples alone. For this reason, sub-sample data for both samples were combined to yield a pooled regression with an apparent age of 791±42 Ma (n=6, MSWD = 11.2; ε_{Ndi} = +0.6±3.7, Fig.7a). A whole rock powder of sample 1 also has high Sm/Nd (i.e. its REE budget is controlled by vein apatite) but plots slightly below the apatite isochron.

By contrast, the U-Pb data are more difficult to interpret. In simple U-Pb isochron diagrams, the data are scattered, in particular for apatites from sample 2 which have lower U/Pb and $^{206}Pb/^{204}Pb$ (<36). Apatites from sample 1 are more radiogenic ($^{206}Pb/^{204}Pb$ up to 202) but still scatter strongly in the $^{206}Pb/^{204}Pb$ vs $^{238}U/^{204}Pb$ plot (Fig. 7b), with an apparent age of 619±130 Ma. Surprisingly, a much better correlation is observed in the $^{207}Pb/^{204}Pb$ vs $^{235}U/^{204}Pb$ plot which yields a precise age of 665±4 Ma (n=4, MSWD = 0.22, $^{207}Pb/^{204}Pbi$ = 16.32±0.05: Fig. 7c). Radiogenic Pb/U ages can be assessed in the Tera-Wasserburg and Wetherill concordia diagrams, but in all cases data are strongly scattered and yield highly imprecise and inconsistent apparent ages in the range 600-850 Ma (not shown). Finally, in the $^{207}Pb/^{204}Pb$ vs $^{206}Pb/^{204}Pb$ diagram, the uranogenic Pb isotope data define a moderately scattered linear array. If this is interpreted as a secondary Pb-Pb isochron, the indicated age is 835 ± 62 Ma (NIF1.1 omitted, n = 7; MSWD = 24; Fig. 7d). It is clear that the apatite U-Pb isotope systems have been disturbed to variable extent and no longer preserve their original age.

In addition to the Sm-Nd/U-Pb data, $^{87}Sr/^{86}Sr$ ratios were measured for 6 of the apatite fractions. As Rb/Sr ratios for Nifty apatites are essentially zero (≤0.00043 for 8 trace element fractions, Table 2), the present-day $^{87}Sr/^{86}Sr$ ratios (0.7214-0.7238) are also initial ratios.

Table 2: Trace element analyses of apatite separates (in ppm)

	NIF1.1	NIF1.2	NIF1.3	NIF1.4	NIF1.5	NIF2.1	NIF2.2	NIF2.3	NIF2.4	NIF2.5
Mg	280	295	602	161	348	49	102	93	69	117
Sc	4.9	7.2	8.7	8.0	11.2	21.7	19.6	18.8	9.8	11.5
Ti	4.5	4.0	3.0	3.5	6.6	1.7	1.0	1.3	1.8	2.2
V	1.2	1.1	2.0	0.6	1.5	0.1	0.1	0.2	0.5	0.5
Cr	0.6	0.1	0.1	0.3	0.3	0.0	0.0	0.6	0.1	0.0
Cu	4,413	136	496	437	439	56	107	282	468	208
Zn	11	89	97	95	165	15	876	462	1,551	2,518
Ga	1.4	1.2	1.7	1.1	1.4	1.1	1.0	1.1	1.1	1.1
Rb	0.04	0.06	0.12	0.04	0.11	0.14	0.15	0.19	0.36	0.37
Sr	411	568	639	686	599	977	884	863	1,004	861
Y	109	129	150	139	132	168	134	145	137	134
Zr	3	0	0	1	2	0	0	0	0	0
Nb	0.03	0.05	0.03	0.04	0.08	0.01	0.01	0.01	0.10	0.01
Ba	188	366	536	496	464	52	39	36	43	44
La	3.19	2.88	3.24	4.04	3.69	12.86	7.66	13.03	9.91	7.50
Ce	18.77	16.34	17.01	20.63	20.56	21.82	14.51	21.16	18.56	16.76
Pr	5.32	4.73	4.88	5.68	5.77	4.28	3.01	4.00	3.52	3.55
Nd	44.39	40.46	41.80	46.90	47.83	33.41	25.12	30.61	26.12	27.31
Sm	52.88	54.03	57.84	59.81	59.51	61.77	50.14	53.04	45.87	45.64
Eu	20.74	21.73	23.51	23.53	23.18	34.19	27.24	27.89	26.15	25.95
Gd	116.3	124.1	135.0	134.3	131.0	169.8	139.3	145.8	125.6	127.2
Tb	12.37	13.72	15.56	14.69	13.87	20.53	16.71	17.42	15.96	15.09
Dy	41.67	46.86	54.49	49.59	47.50	67.59	55.52	58.50	54.95	52.36
Ho	5.07	5.88	6.88	6.22	5.88	8.20	6.58	7.03	6.74	6.32
Er	8.58	10.37	12.15	11.23	10.37	14.27	11.75	12.33	12.04	11.51
Tm	0.79	1.04	1.23	1.13	1.05	1.49	1.21	1.26	1.28	1.21
Yb	3.61	5.06	5.89	5.57	5.13	7.33	5.99	6.20	6.37	6.00
Lu	0.37	0.54	0.61	0.59	0.57	0.80	0.66	0.65	0.69	0.65
Hf	0.08	0.04	0.05	0.05	0.07	0.04	0.04	0.03	0.04	0.03
Ta	0.01	0.01	0.00	0.00	0.01	0.01	0.00	0.01	0.00	0.01
Pb	12.76	32.41	24.25	52.35	67.47	7.86	4.83	171.19	8.51	24.24
Th	0.31	0.12	0.31	0.10	0.18	0.96	0.36	0.16	0.34	0.51
U	101.18	143.99	140.29	151.00	233.74	35.50	20.54	51.53	26.81	45.40

Implications of results

AGE OF MINERALISATION

The isotopic data presented here suggest that apatites from the Nifty deposit record a complex geological history. Based on the uniform apatite REE patterns (which suggest formation from fluids with similar REE content and thus, presumably, uniform initial $^{143}Nd/^{144}Nd$), the pooled Sm-Nd age of 791±42 Ma is considered the most reliable estimate of vein formation available at present. This pooled age is consistent with the similar but less precise age for the 3 apatite fractions from sample 1 alone (MSWD 1.05, 810±100 Ma, ε_{Ndi} = -0.6). Further confirmation of a ca. 800 Ma apatite age is derived from modelling of initial ε_{Nd} values (Fig. 8). Due to their very high Sm/Nd ratios ($^{147}Sm/^{144}Nd$ = 0.7-1.0), calculated initial ε_{Nd} values for the apatites are very sensitive to small changes in assumed age (0.7-0.85 ε_{Nd} units for every 10 Ma, equivalent to 2x analytical precision).

By comparison, crustal rocks with Sm/Nd near the crustal average ($^{147}Sm/^{144}Nd \sim 0.110$) are much less sensitive to age corrections; in such rocks, ε_{Ndi} changes by about 1 unit/100 Ma. Calculated initial ε_{Nd} for the apatites must be consistent with ε_{Ndi} in reservoirs available within the "elemental catchment" of the hydrothermal parent fluids, i.e. the Broadhurst Fm and/or other lithologies in the Throssell Range Group and wider Paterson Orogen. At ca. 800 Ma, our preferred vein-forming age, apatite ε_{Ndi} range from -1.2 to +0.1. At 830 Ma, the apatite ε_{Ndi} range shifts to -1.9 to -4.4. Through the same age range, ε_{Ndi} in various lithologies in the Throssell Range Group (Coolbro Sandstone, Broadhurst Formation) varies from -8 to -10. Limited data for the much older gneisses and granitoids in basement of the Rudall Complex indicates ε_{Ndi} near 800 Ma of about -16 (McCulloch, 1987; Maas and Bagas, in prep; Geoscience Australia, unpubl. data). By comparison, for any age <750 Ma, ε_{Ndi} in the apatites are all positive (+3 to +6), while ε_{Ndi} in possible source reservoirs becomes more negative. Assuming that Sm-Nd isotope systematics of the vein apatites remained undisturbed during the events recorded by the U-Pb system, the ε_{Ndi} systematics of the apatites appear to preclude any formation age substantially younger than 800 Ma. On the other hand, substantial overlap of ε_{Ndi} in the apatites and lithologies in the Throssell Range Group only occurs for ages >850 Ma.

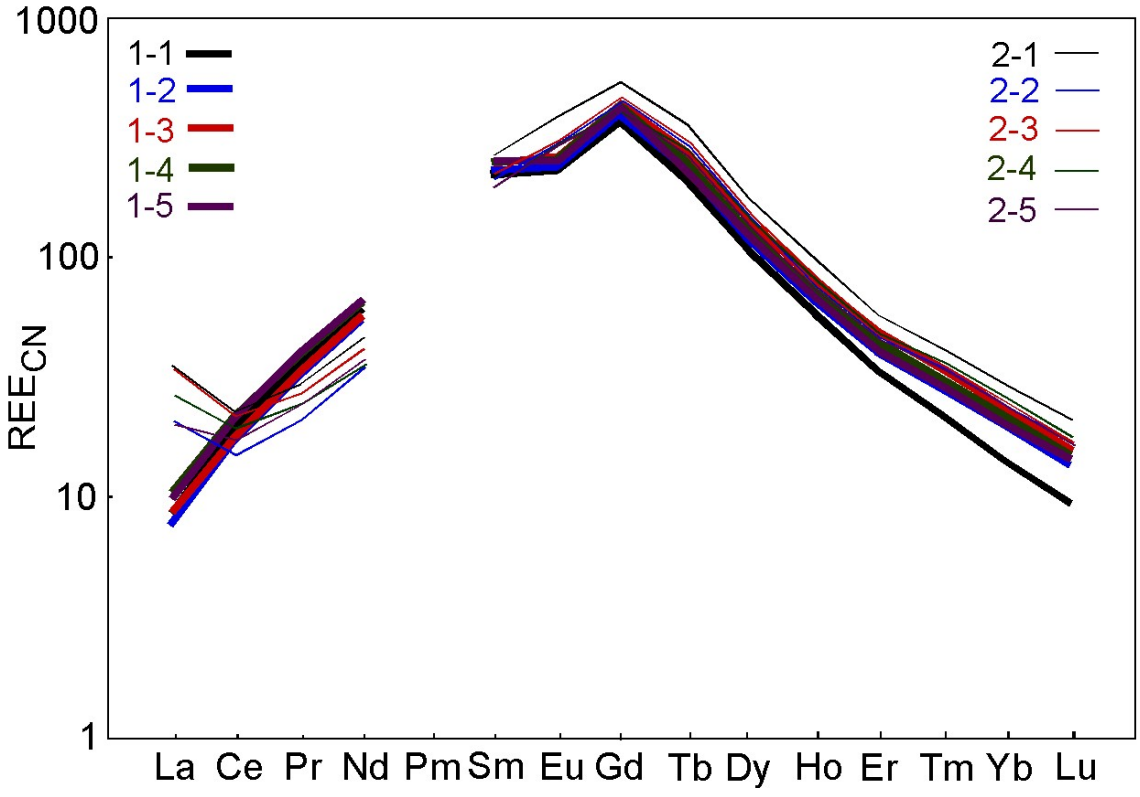

Figure 6: *Chondrite-normalised rare-earth element patterns for apatite grains from the Nifty deposit.*

Table 3: Sm-Nd and Sr isotope results

	Sm (ppm)	Nd (ppm)	$^{147}Sm/^{144}Nd$	$^{143}Nd/^{144}Nd$	ε_{Ndnow}	$^{87}Sr/^{86}Sr$	ε_{Ndi}
NIF1.1ap	55.36	44.80	0.7471	0.515529	56.40	0.72214	+0.8
NIF1.2ap	55.26	46.65	0.7161	0.515353	52.97	0.72264	+0.5
NIF1.3ap	59.37	51.16	0.7016	0.515291	51.76	0.72136	+0.7
NIF1.4ap						0.72314	
NIF2.1ap	39.45	23.41	1.0188	0.516890	82.93	0.72389	-0.1
NIF2.2ap	41.40	23.42	1.0689	0.517249	89.94	0.72377	+1.8
NIF2.3ap	35.83	21.26	1.0188	0.516901	83.15		+0.1
NIF1ap	20.93	15.60	0.8109	0.515682	59.39		-2.7

Sm, Nd in ppm; all Nd isotope data adjusted to La Jolla = 0.511860; BCR-1 $^{147}Sm/^{144}Nd$ =0.1380(±0.14%), $^{143}Nd/^{144}Nd$ = 0.512645 (±0.0046%). External precision (2sd) is 0.004% for $^{143}Nd/^{144}Nd$, 0.2% for $^{147}Sm/^{144}Nd$;
External precision for $^{87}Sr/^{86}Sr$ ±0.00003 (2sd), data adjusted to SRM987 = 0.71023. Measured apatite $^{87}Sr/^{86}Sr \approx$ initial $^{87}Sr/^{86}Sr$ due to extremely low Rb/Sr (see text); CHUR is 0.1967, 0.512638; ε_{Ndi} is deviation from CHUR in 0.1‰ units at 790 Ma; $\lambda^{147}Sm=6.54x10^{-12}a^{-1}$

The U-Pb systematics are clearly disturbed and record a complex pattern of changes in Pb/U ratios. This may have taken place via diffusional mechanisms but could also be explained by a combination of initial Pb isotope heterogeneity (possibly preserved in sulphide inclusions) and later redistribution of Pb by renewed sulphide formation. The possible presence of disseminated uraninite (see above) is an additional factor because of the tendency of this mineral to recrystallise and release highly radiogenic Pb to local pore fluids (Cumming and Krstic, 1992; Evins et al., 2005). It seems unlikely that any of the U-Pb or Pb-Pb ages date particular events, although the apparent bracketing of these ages between the Sm-Nd isochron age (near 800 Ma) and ca. 600 Ma suggests the disturbance in the U-Pb data may be related to the thermal/fluid event related to the ca. 650 Ma Miles Orogeny.

Table 4: U-Pb isotope results

	U (ppm)	Pb_t (ppm)	Pb_c (ppm)	$^{238}U/^{204}Pb$	$^{206}Pb/^{204}Pb$	$^{207}Pb/^{204}Pb$	$^{208}Pb/^{204}Pb$
NIF1.1ap	240.0	36.49	13.9	1055 (0.28)	123.9 (0.21)	23.40 (0.30)	37.93 (0.40)
NIF1.2ap	89.3	29.29	18.2	300.7 (0.26)	57.09 (0.20)	18.33 (0.30)	37.89 (0.40)
NIF1.3ap	81.9	10.99	2.91	1725 (0.37)	202.0 (0.28)	27.87 (0.33)	38.02 (0.42)
NIF1.4ap	116.1	27.86	15.0	473.9 (0.25)	73.55 (0.20)	19.48 (0.30)	37.90 (0.40)
NIF2.1ap	16.23	22.23	17.2	57.89 (0.25)	36.13 (0.20)	16.72 (0.30)	38.02 (0.40)
NIF2.2ap	12.83	15.98	12.7	62.07 (0.25)	33.98 (0.20)	16.57 (0.30)	38.04 (0.40)
NIF2.3ap	17.31	12.74	10.1	104.7 (0.25)	33.61 (0.20)	16.58 (0.30)	38.03 (0.40)
NIF2.4ap	16.38	114.6	105.6	9.62 (0.34)	23.00 (0.20)	16.01 (0.30)	37.90 (0.40)

U in ppm; Pb_t is total Pb in ppm; Pb_c is common Pb in ppm, based on an arbitrarily chosen common Pb from Stacey-Kramers growth curve at 850 Ma; all ratios are atomic, with 2s% in brackets. $^{238}U/^{235}U$ = 137.88

The simplest interpretation of these data is that the Nifty deposit formed close to the timing of sedimentation, either syngenetically or diagenetically, and was recrystallised and remobilised into the present, largely structurally controlled, site during the Miles Orogeny. It is possible that the

original sulphide deposit localised the Nifty Syncline and that the ores were redistributed into their present site during localised deformation and fluid flow during the Miles Orogeny (c.f. Czarnota, 2006). Although the broad location of the deposit was determined during sedimentation, structural factors are important controls on the present distribution of ore, particularly high grade pods.

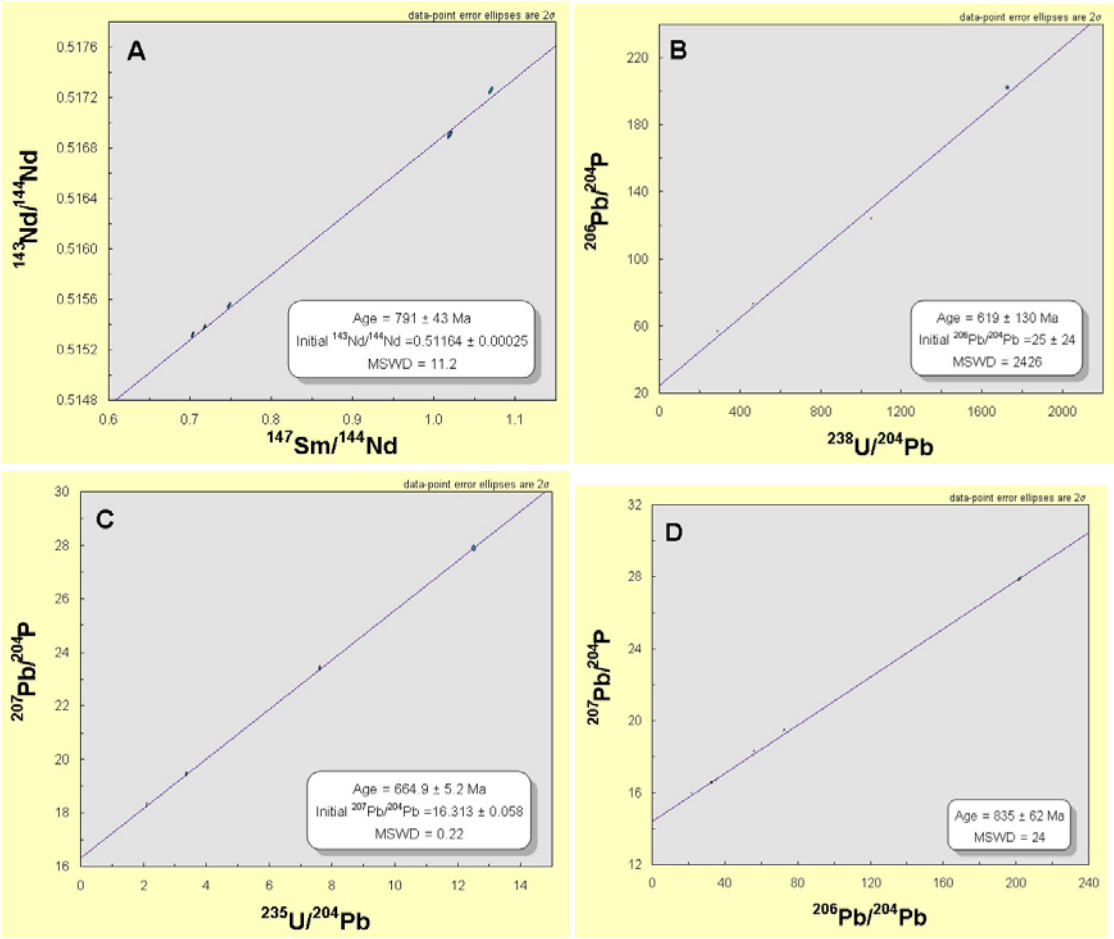

Figure 7: *Plots showing isochrons and errorchrons based on apatite analyses from samples 2005678048-01 and 2005678051-02. (A) $^{147}Sm/^{144}Nd$ versus $^{143}Nd/^{144}Nd$ diagram showing isochron for all analyses. (B) $^{238}U/^{204}Pb$ versus $^{206}Pb/^{204}Pb$ diagram showing all analyses. (C) $^{235}U/Pb^{204}$ versus $^{207}Pb/^{204}Pb$ diagram showing isochron established from analyses from sample 2005678048-01. (D) $^{207}Pb/^{204}Pb$ versus $^{206}Pb/^{204}Pb$ diagram showing errorchron generated for all analyses less one outlier.*

ISOTOPIC CONSTRAINTS ON FLUID AND METAL SOURCES

Initial isotopic ratios, the crystallinity of disordered carbon, the character of primary fluid inclusions, sulphur isotope data and the presence of high uranium contents in the apatite veins also provide important constraints on the character of the ore fluids. The initial ε_{Nd} of the apatite isochron (+0.6±3.7, the unusually large error is due to lack of low-Sm/Nd points on the isochron, resulting in unfavourable extrapolation of the error envelope to the y-axis) is higher than ε_{Ndi} in Yeneena Group sediments and Rudall Complex crystalline basement (≤ -10). In fact, none of the rock units for which

Nd isotope data are currently available, including the Duke Monzonite, have ε_{Ndi} values consistent with those from Nifty apatite. Other possible, though untested, sources for the Nd are ca. 830 Ma mafic sills that intrude most units within the Paterson region and Paleoproterozoic ultramafic rocks that intrude the Rudall Complex.

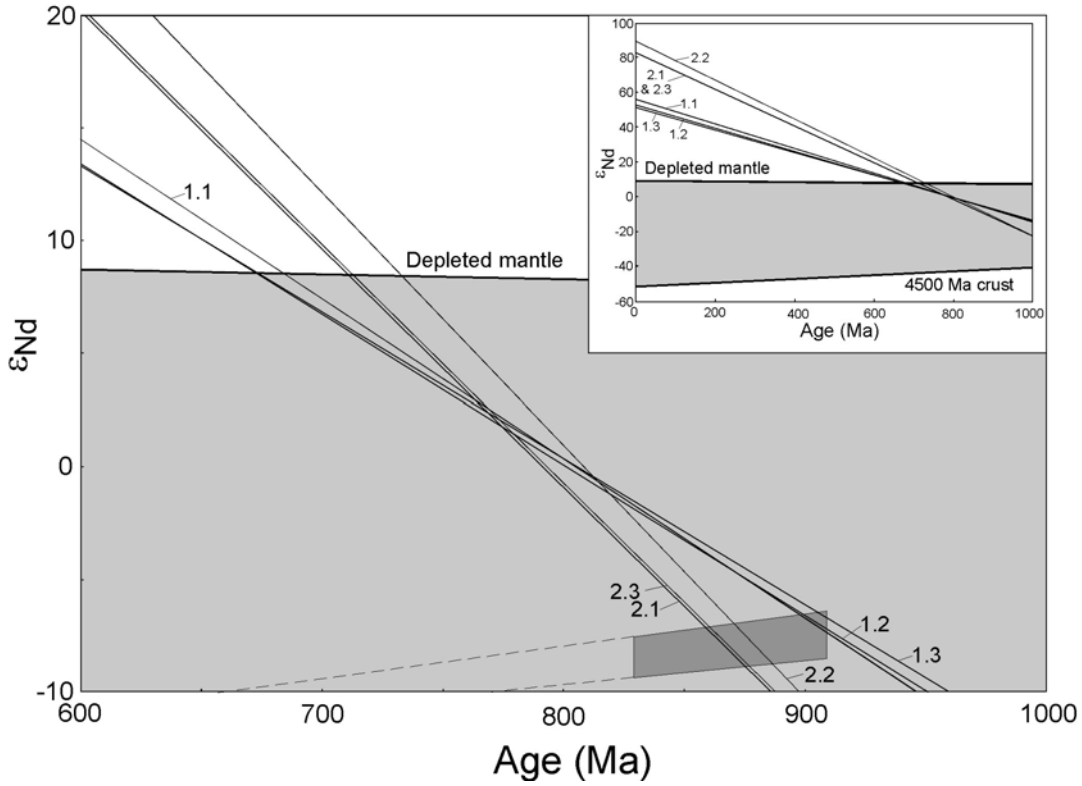

Figure 8: *Diagram showing the evolution of ε_{Nd} back through time in comparison with evolution curves of depleted mantle and continental crust extracted from the mantle at 4500 Ma. The light gray field shows theoretically permitted ε_{Nd} values. The dark gray field indicates ε_{Nd} values of the Throssell Group at the time of deposition. The dashed lines from this field to younger ages indicate the ε_{Nd} evolution of these rocks with time.*

Alternatively, if mineralisation is older than ≈800 Ma, the gap between apatite and Yeneena group sediments is narrowed. For example, if the apatite data are paired with Sm-Nd data for Yeneena Group samples (R. Maas and GA, unpubl. data), apparent ages in the range 860-914 Ma are obtained, with initial ε_{Nd} near -8. While still within the range of likely depositional ages for the Broadhurst Fm (910-830 Ma), such older ages produce initial ε_{Nd} that can be explained by equilibration of the hydrothermal fluids with local host rocks. Obviously, the low ε_{Nd} values obtained in such regressions is the direct result of using the Yeneena Nd data. The justification for pairing Nifty apatite and Yeneena Nd data in preference to using only data for the apatite becomes critical for any further discussion of both age and fluid source.

One further observation must be mentioned: the detailed Nd isotope systematics in the analysed samples indicates resolvable isotopic disequilibrium between the various apatite fractions, and between the three sample 1 apatites and their matrix (NIF1wr). Disequilibrium in sample 1 is particularly noticeable, with NIF1wr yielding ε_{Ndi} between 2-3 units lower than the corresponding apatites at all reasonable ages. Unless this is an artefact of post-depositional disturbance, it would indicate that pure hydrothermal material has a slightly more radiogenic Nd isotope signature than its immediate host rock. NIF1wr is in turn more radiogenic than Yeneena Group sediments (incl Broadhurst Fm) remote from mineralisation (ε_{Ndi} of -2.7 vs ≈-9 at 790 Ma). This would imply that mineralisation involved fluids with an imported Nd component derived from sources with high ε_{Nd}, such as the 830 Ma mafic sills mentioned earlier.

In contrast to the Nd isotope evidence, the initial $^{87}Sr/^{86}Sr$ of the apatites (~0.722) is perfectly compatible with a Sr source in Yeneena Group sediments, as well as in Rudall Complex basement rocks. For example, two samples of Coolbro Sandstone have $^{87}Sr/^{86}Sr_{800}$ near 0.720, very similar to the apatite signature. The latter is insensitive to the exact apatite age. This generates an interesting situation: Sr isotopes indicate an evolved (high-Rb/Sr) source whereas Nd isotopes indicate a more primitive (high ε_{Nd}, usually associated with low $^{87}Sr/^{86}Sr$) source. This apparent contradiction may be the consequence of source type and degree of source leaching. Sr is highly mobile in crustal fluids (e.g. Negrel et al 1997; Davies et al., 1998) and will be readily leached from the dominant rock types in contact with the hydrothermal fluid. As noted above, lithologies with high $^{87}Sr/^{86}Sr_{800}$ would have been common within the Neoproterozoic Throssell Group and the Mesoproterozoic Rudall Metamorphic Complex. In fact, equilibration with the local host rocks, a sequence of dolomitic and carbonaceous mudstones, is probably sufficient to produce the apatite Sr isotope signature. By contrast, the rare earths, incl. Nd, are relatively immobile unless water/rock ratios are high (e.g. Michard, 1989). However, glassy or microcrystalline mafic volcanic rocks emplaced within the sediment pile might be a more readily leachable source of mobile REE's. A source of this nature might explain both the high apparent ε_{Nd} and the high Cu content of the ore fluids. Mantle-derived volcanics are more enriched in Cu than continental sediments and thus would make a better Cu source. For example, it is widely accepted that the Eastern Creek Volcanics, a thick series of tholeiitic basalts in the western Mt Isa Inlier, was the source of Cu for the massive Mt. Isa Cu deposit (Hannan et al., 1993; Heinrich et al., 1995).

ORE FLUID COMPOSITION

The low vapour/liquid ratios and daughter halite crystals in primary fluid inclusions from the apatite veins suggest that the ore fluids were relatively low temperature and saline. The inference on temperature is supported by laser Raman analyses of disordered carbon. Moreover, this ore fluid was

likely oxidised as indicated by the presence of uranium in the apatite veins, and by the large range in $\delta^{34}S$ values of ore-related pyrite and chalcopyrite (-12‰ to 6‰: Anderson et al., 2001). Furthermore variation in Ba content may be an indication of varying redox conditions during deposition. These data and the radiogenic isotope results suggest that the Nifty (and by implication Maroochydore) deposits were deposited diagenetically or syngenetically from oxidised, relatively low temperature basinal brines, with copper derived from mafic sills in the host package. This work, our previous work and geochemical data provided by Nifty Birla suggest that the Nifty ores in part replaced carbonate beds within a sequence dominated by carbonaceous shales and siltstone. It is likely that ore deposition occurred as a consequence of reduction of the ore fluids to the pyrite stability field by reaction with carbonaceous material in the host units. The association with carbonate also suggests that a coincident increase in pH was also important for ore deposition. These results suggest that the critical factors in forming the Nifty deposit are mafic or ultramafic rocks as a copper source; oxidised, low temperature basinal brines; and the presence of carbonate lenses within an overall reduced, carbonaceous shale-siltstone rock package. The Miles Orogeny potentially upgraded the orebody, mobilising it into its present position. This model is consistent with the original WMC exploration model as described in Haynes et al. (1993) but less consistent with the current syn-tectonic model described by Anderson et al. (2001). The presence of uranium within the Nifty deposit may suggest a broad relationship to the hydrothermal systems that formed uranium deposits in the Paterson, including the Kintyre deposit.

STRUCTURAL IMPLICATIONS AND VECTORS TO MINERALISATION

The weight of geochronological evidence indicates either a syngenetic or digenetic formation of the Nifty ore deposit. This raises questions with respect to the type of structures which focused fluid flow during the formation of the deposit. The natural structural candidates are early normal faults associated with Yeneena Basin formation. If this is correct ore trends would lie parallel to these faults or within breached relay ramps. This section examines the likely orientation of these early normal faults and their associated ore trends within now folded Yeneena Basin.

The NNW striking Vines Fault (Fig. 1) is inferred to be a master early basin bonding growth fault. From the clear strike of the Vines Fault the orientation of second and third order normal synthetic and antithetic structures during the formation of the Yeneena Basin can be inferred to be NNW striking and therefore potential effects of folding during the Miles Orogeny on these structures can be established.

To establish the current orientation of these inferred early normal faults hypothetical synthetic and antithetic normal faults striking 340˚ and dipping 60˚ east and west respectively have been folded

based on the orientation of the two limbs of the Nifty Syncline (Fig. 9). The results of the folding exercise indicate folded synthetic normal faults would strike NE-SW on the SW dipping limb of the Nifty Syncline and NNW-SSE on the SW dipping limb. These orientations do not correspond with any known ore trends at Nifty. However folded antithetic faults would strike NNW-SSE on SW dipping limbs coincident with the high grade ore trends at Nifty (Fig. 10). On NE dipping limbs the antithetic normal faults would strike NE-SW. When this ore trend orientation is examined on the SW side of the syncline along the NE dipping limb a poorly defined ore trend is highlighted. There are currently three drill holes in this position all with intercepts of greater then 3% Cu (Fig. 9). Due to the sparsity of drilling in this location the Leapfrog Nifty model did not link these areas up with the central high grade ore region, so this trend is still open.

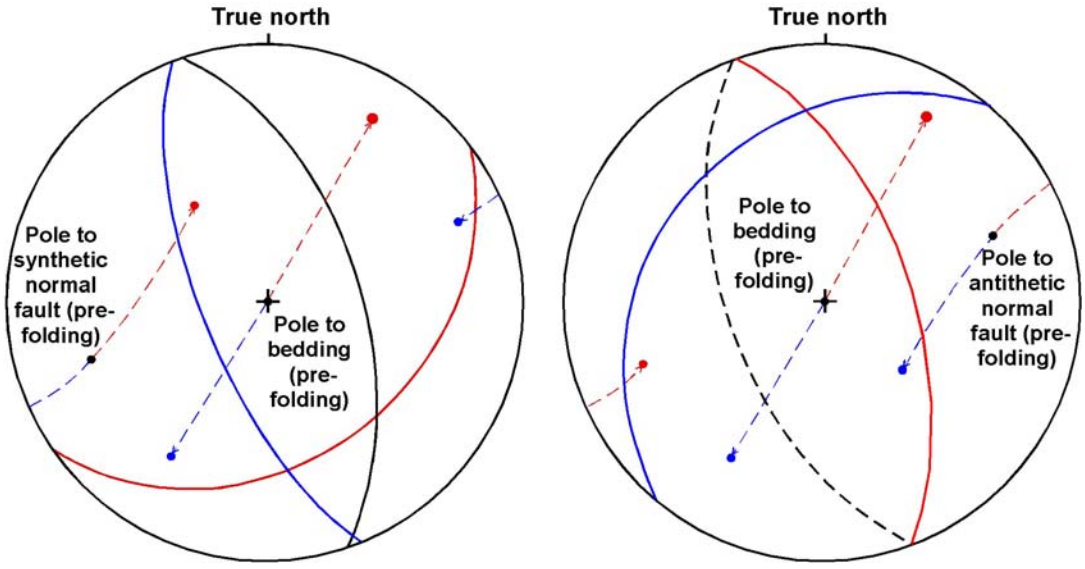

Figure 9: *Folding of inferred (A) synthetic (E dipping) and (B) antithetic (W dipping) normal faults with respect to bedding associated with the formation of the Nifty Syncline. Blue and red girdles represent trend of folded normal faults on NE and SW dipping fold limbs respectively. NB the above assumes negligible plunge of Nifty Syncline since in the ore position the plunge of the fold is horizontal.*

The co-incidence of high grade ore shells and the inferred trend of antithetic normal faults with respect to the basin bonding Vines Fault indicate the strong possibility that the Nifty deposit was controlled by basin formation related normal faults. Due to the Miles Orogeny remobilisation of Cu it may be hard to pick these early structures within the deposit. However this analysis highlights the importance of considering the effects of these early structures on major ore trends.

Conclusions

A paragenetic and geochronology study of chalcopyrite-bearing apatite veins associated with the Nifty copper deposit in the Paterson orogen indicates:

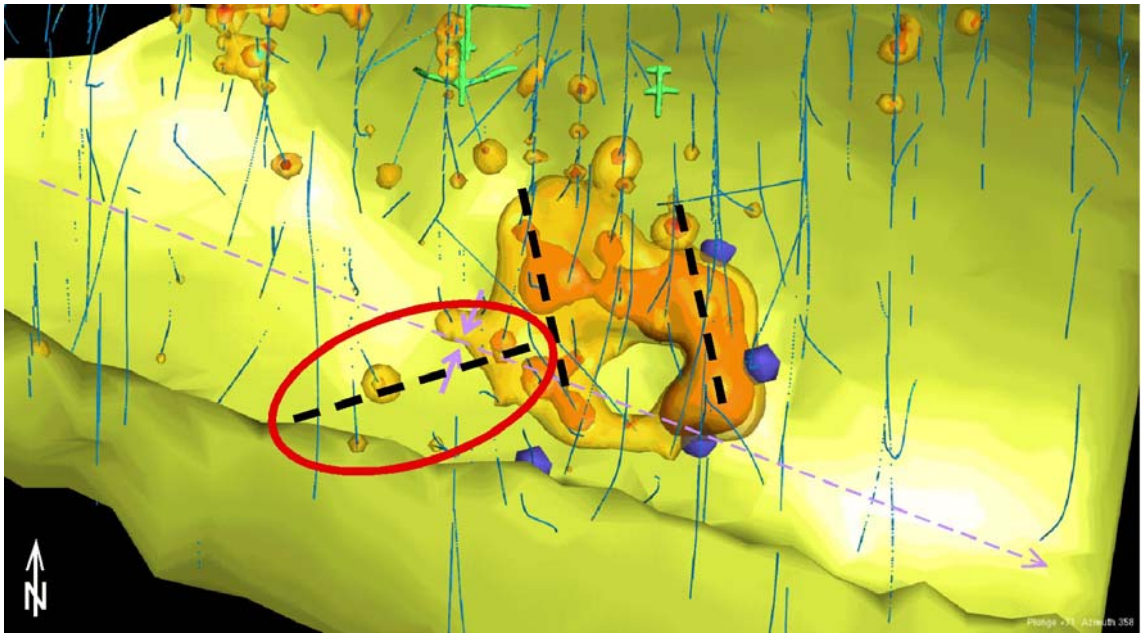

Figure 10: *Oblique plan view of 3% and 5% copper isosurfaces (oranges) on footwall shale unit (yellow), drill hole locations and location of apatite samples. Black dashed lines highlight the NNW-SSE high grade ore trends on the SW dipping limb of the fold and the possible NE-SW trend on the NE dipping fold limb. Red ellipse outlines the possible extension of high grade mineralisation on the SW side of the Nifty syncline as per the antithetic folded normal fault model.*

- Apatite in the apatite veins is paragenetically associated with copper mineralisation.
- The apatite veins were folded after deposition of the Nifty ores.
- A Sm-Nd isochron for apatite indicates an age of 791 ± 42 Ma, which is interpreted as the age of mineralisation.
- The U-Pb system has been disturbed, possibly during deformation and fluid flow associated with the Miles Orogeny at ca. 650 Ma.
- Observations of primary fluid inclusions, in combination with the geochronology data and sulphur isotope data suggest that the ores formed from oxidised, low temperature fluids.
- Nd isotope data may indicate a relatively primitive source for hydrothermal Nd, possibly through leaching of ca. 830 Ma mafic sills.
- Sr isotope data, however, indicate a relatively evolved source for Sr, consistent with sourcing from sedimentary rocks within the Yeneena basin.
- Structural modelling assuming early (i.e. pre-tectonic) copper mineralisation suggests that ore trends on the northeast side of the Nifty syncline are consistent with control of antithetic normal faults formed during the formation of the Yeneena basin. If this is correct, these faults should trend west-southwest on the southwest limb of the Nifty syncline.

These results are consistent with the genetic model of Haynes et al. (1993) and less consistent with the model of Anderson et al. (2001).

REFERENCES

Author, A. A., Author, B. B., Author, C. C, Author, D. D. and Author, E. E., 2004. Reference Title. *Geoscience Australia Record,* **2005/xx**, 109pp.

Anderson, B. R., Gemmell, J. B. and Berry, R. F., 2001. The geology of the Nifty copper deposit, Throssell Group, Western Australia: implications for ore genesis. Economic Geology, **96**, p. 1535-1565.

Bagas, L., 2004. The Neoproterozoic Throssell Range and Lamil Groups, northwest Paterson Orogen, Western Australia - a field guide. Geological Survey of Western Australia Record, **2004/15**, 18pp.

Beyssac, O., Goffé, B., Chopin, C. and Rouzaud, J.N., 2002. Raman spectra of carbonaceous material in metasediemnts: a new geothermometer: Journal of Metamorpyic Geology, **20**, p. 859-871.

Cumming, G. L. and Krstic, D., 1992. The age of unconformity-related uranium mineralization in the Athabasca Basin, northern Saskatchewan. Canadian Journal of Earth Sciences, 29, p. 1623–1639.

Czarnota, K., 2006. Nifty district numerical modelling: preliminary results and some predictive targeting outcomes. Unpub. report to Nifty-Birla, 9pp.

Davies, J. F., Prevec, S. A., Whitehead, R. E. and Jackson, S. E., 1998. Variations in REE and Sr-isotope chemistry of carbonate gangue, Castellanos Zn-Pb deposit, Cuba. Chemical Geology, **144**, p. 99-119.

Dunphy, J. M. and McNaughton, N. J., 1998. Geocchronology of the Telfer granitoids: zircon and titanite U-Pb SHRIMP data. Geological Society of Asutralia Abstracts, **49**, p. 127.

Durocher, K. E., Kyser, T. K., Marlatt, J. and Hanly, A., 2002. New $^{40}Ar/^{39}Ar$ ages from the central Paterson Orogen, Western Australia. Australian Journal of Earth Sciences, **50**, p. 601-610.

Eggins, S. M., Woodhead, J. D., Kinsley, L. P. J., Mortimer, G. E., Sylvester, P., McCulloch, M. T., Hergt, J. M. and Handler, M. R., 1997. A simple method for the precise determination of ≥40 trace elements in geological samples by ICPMS using enriched isotope internal standardisation. Chemical Geology, **134**, p. 311-326.

Evins, L. Z., Jensen, K. A. Ewing, R. C., 2005. Uraninite recrystallization and Pb loss in the Oklo and Bangombé natural fission reactors, Gabon. Geochimica et Cosmochimica Acta, **69**, 1589-1606.

Goellnicht, N., 1992. Late Proterozoic fractionated granitoids and their role in the genesis of gold and base-metal the mineralisation in the Telfer district, Western Australia. Unpub. Ph.D. thesis, University of Western Australia.

Hannan, K. W., Golding, S. D., Herbert, H. K. and Krouse, H. R., 1993. Contrasting alteration assemblages in metabasites from Mount Isa, Queensland: implications for copper ore genesis. Economic Geology, **88**, p. 1135-1175.

Haynes, D. W., Brooke, W. J. L., and Mazzoni, P. P., 1993. Application of conceptual models for sediment-hosted ore deposits in the discover of the Nifty copper and adjacent zinc-lead deposits, Yeneena basin, Western Australia. Geological Association of Canada Special Paper, **40**, p. 75-88.

Heinrich, C. A., Bain, J. H. C., Mernagh, T. P., Wyborn, L. A. I., Andrew, A. S. and Waring, C. L., 1995. Fluid and mass transfer during metabasalt alteration and copper mineralization at Mount Isa, Australia. Economic Geology, **90**, p. 705-730.

Kamber, B. S., Greig, A., Schönberg, R. and Collerson, K. D., 2003, A refined solution to Earth's hidden niobium: implications for evolution of continental crust and mode of core formation. Precambrian Research, **126**, p. 289-308.

Maas, R., Kamenetsky, M. B., Sobolev, A. V., Kamenetsky, V. S. and Sobolev, N. V., 2005. Sr-Nd-Pb isotopic evidence for a mantle origin of alkali chlorides and carbonates in the Udachnaya kimberlite, Siberia. Geology, **35**, p. 549-552.

Maas, R. and Bagas, L., in prep., The Kintyre U-deposit, Paterson Orogen, Western Australia: U-Pb and Sr-Nd isotopic constraints on the genesis of a large unconformity-type U deposit and its link to sedimentary sequences of the Neoproterozoic Centralia Superbasin.

McCulloch, M. T., 1987. Sm-Nd isotopic constraints on the evolution of Precambrian crust in the Australian continent, in Kröner, A. (ed.) Proterozoic Lithospheric Evolution. Geodynamics Series, **17**, p. 115-145.

Michard, A., 1989. Rare earth element systematics in hydrothermal fluids: Geochimica et Cosmochimica Acta, **53**, p. 745-750.

Negrel, P., Fouillac, C. and Brach, M., 1997. A strontium isotopic study of mineral and surface waters from Cezallier (Massif Central, France): implications for mixing processes in areas of disseminated emergences of mineral waters. Chemical Geology, **135**, p. 89-101.

Nelson, D., 1995. Compilation of SHRIMP U-Pb zircon geochronology data, 1994. Geological Survey of Western Australia Record, **1995/3**, 244pp.

Reed, A., 1996. The structural, stratigraphic and temporal setting of the Maroochydore copper prospect, Paterson orogen, Western Australia. Unpublished Ph.D. thesis, Perth, Australia, University of Western Australia, 289pp.